Domain Coarsening in a Two-Dimensional Binary Mixture: Growth Dynamics and Spatial Correlations

Michael Seul, Nicole Y. Morgan,* and Clément Sire†
AT&T Bell Laboratories, Murray Hill, NJ 07974
(Received 16 May 1994)

Late-stage coarsening in a 2D binary mixture has been investigated via direct imaging of "bubble" domains in an amphiphilic monolayer at an air-water interface. In a regime with growth exponent $n \simeq 0.28$ for the mean domain radius, the radius distribution exhibits dynamic scaling, closely approaching a Gaussian shape. The local structure of disordered bubble patterns ensures short-range screening of topological charge. Pattern statistics correspond to equilibrated random Voronoi lattices and indicate a prominent role of entropy maximization. Pattern stabilization against bubble coalescence is attributed to electrostatic interactions.

PACS numbers: 05.70.Ln, 64.60.−i, 64.75.+g, 75.70.Kw

The domain coarsening which mediates the approach to equilibrium in systems subjected to a rapid field or temperature quench has received a great deal of experimental and theoretical attention [1]. A central topic of theoretical interest has been the incorporation of interdomain correlations in the analysis of the growth dynamics. Neglected in the classic mean-field treatments of systems with conserved order parameter [2], diffusion mediated correlations are in fact relevant in the presence of a finite fraction of minority phase [3], a common experimental situation. Theoretical progress [4], especially in the analysis of two-dimensional systems [5,6], has led to the prediction that, while preserving an asymptotic scaling state characterized by a growth exponent of $\frac{1}{3}$ for the mean droplet radius, correlations greatly affect the functional form of the universal distribution; in addition, such correlations are expected to induce spatial correlations in the configuration of domains. While a variety of simulations have addressed these aspects of the coarsening dynamics [3,7], experiments relying on direct imaging of suitable two-dimensional systems are only now beginning to appear [8].

We report here on the late-stage domain coarsening ("ripening") in a two-dimensional binary mixture, formed by immiscible liquid phases of two amphiphiles within a monomolecular film at an air-water interface. Extensive pattern analysis of fluorescence images, recorded following isothermal quenches in surface pressure for "off-critical" mixtures, yields not only the growth law $\langle A \rangle \sim t^{2n}$, for the mean droplet area, with $n \sim 0.28$ over 3 orders of magnitude in time, but also the complete droplet radius distribution $P(R/\langle R \rangle)$: This is shown to exhibit a universal shape closely approximated by a Gaussian. Coarsening droplet patterns retain a high concentration of topological defects $N_{n\neq 6}/N \geq 0.5$, and the application of Voronoi analysis reveals their geometrical and topological statistics to display remarkably detailed analogies to space filling cellular patterns ("froths") [9]. In particular, coarsening droplet patterns exhibit a pronounced anticorrelation between the area of a given droplet and the mean area of droplets in its nearest neighbor (NN) shell: The nature of this correlation is such that topological charge is virtually completely screened at the scale of NN distances. Invoking the notion that maximization of entropy controls the configurations of the evolving patterns, we provide a quantitative account of this observation. We attribute the stabilization of the local pattern structure to the suppression of droplet coalescence by repulsive interdomain interactions.

Langmuir films, formed by a mixture of dimyristoylphophatidylcholine and dihydrocholesterol [10], with molar ratio 80:20, corresponding to an area fraction of minority phase $\phi \simeq 0.25$ [11], were equilibrated in their uniform phase [10,12] at 19 °C. They were then subjected to rapid (mechanical) expansion, typically in the range of molecular areas $A_{\text{init}} \sim 61$ Å^2 to $A_{\text{final}} \sim 67$ Å^2. Off-critical values for the composition were chosen so as to avoid crossing the stripe phase regime in the vicinity of the critical mixing point [12–14] and to ensure the nucleation of circular bubble domains. The coarsening dynamics were monitored for up to $\simeq 90$ h following layer expansion, by relying on computer controlled time-lapse video recording. Image analysis procedures are described elsewhere [14].

The temporal evolution of the mean droplet area $\langle A \rangle$ is shown in Fig. 1 for three different runs. Linear fits to the power-law regime yield a value of $n = 0.28 \pm 0.01$ for the exponent in the growth law $\langle A \rangle \sim t^{2n}$ [15]. The initial portion of each of the plots in Fig. 1, controlled by the fastest growing unstable mode in the concentration field [7], yields an estimate of 40 μm^2 for the area, or 3.5 μm for the radius of the critical nucleus. Intercepts of the linear fits to the power-law regime yield values for the rate of growth of the mean *radius*, $k \equiv \langle R \rangle / t^n$, in the range $\sim 0.38 \leq k \leq 0.43$ μm/min$^{1/3}$, which compares rather well with an expression for k given by Marqusee [16]. The low values of the (bare) line tension appear to be particularly adverse to rapid growth. Droplet coalescence is exceedingly rare: In fact, mutual droplet repulsion, expected in the presence of electrostatic dipolar interactions between domains [17], is clearly evident in the presence of

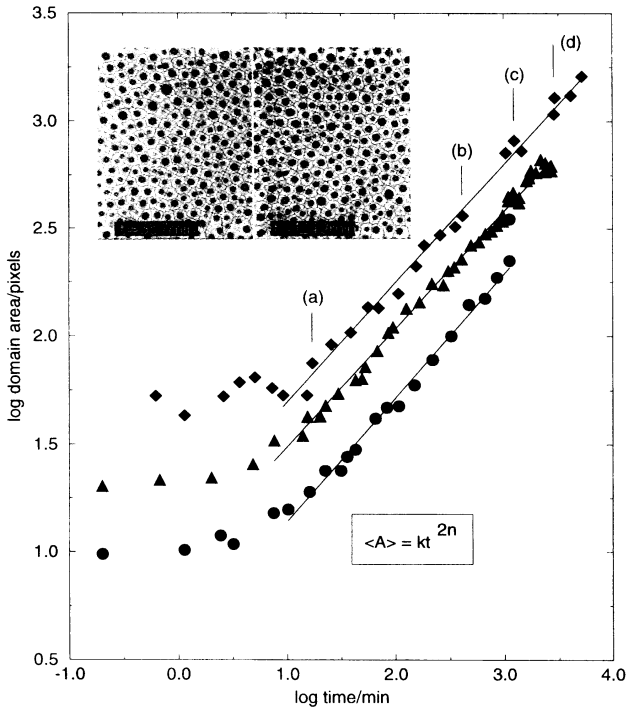

FIG. 1. Domain coarsening. Temporal evolution of mean domain area $\langle A \rangle$ for three runs at composition 80:20, corresponding to $\Phi \sim 0.25$, at temperature 19 °C and approximate surface pressure $\pi \simeq 6$ dyn/cm. Vertical offsets were applied to the middle (-0.25) and bottom (-0.50) graphs. The conversion factor for area units is 10 pixels $\equiv$ 12.4 μm^2. Solid lines represent linear fits which determine the growth exponent (see text). Labels (a)–(d) refer to respective graphs in Fig. 2 below. Inset: Snapshots of (portions of flat-fielded [14]) domain patterns at different stages of coarsening taken from the run, corresponding to the top plot; the corresponding Voronoi diagrams are superimposed. Note the different scales: the black label box represents 150 μm (left panel) and 240 μm (right panel), respectively.

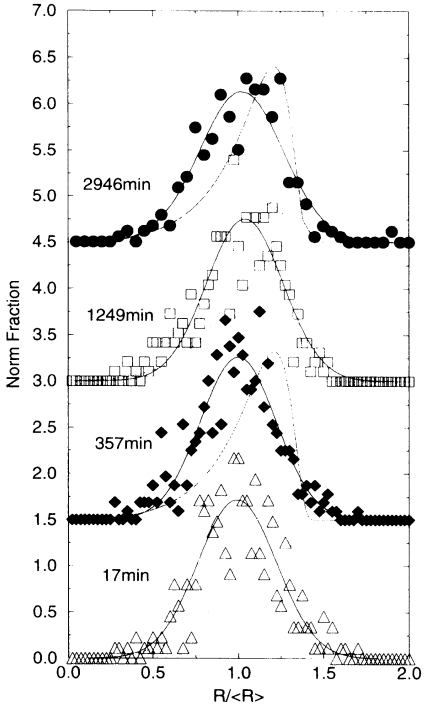

FIG. 2. Normalized scaled domain radius distributions. Typically 250–400 scaled domain radii $R/\langle R \rangle$ per image were collected into 100 bins spanning the interval $[0, 2.5]$. Gaussian fits (solid lines) yield the following sets of optimal parameters for (a)–(d), respectively; $\langle \rho \rangle \equiv \langle R/\langle R \rangle \rangle$:0.99, 1.00, 1.04, 1.02, and σ:0.229, 0.221, 0.224, 0.246; peak amplitudes fall within 1% of the expected value $1/\sqrt{2\pi\sigma}$. A 2D version of the Lifshitz-Slyozov distribution (dashed lines) is also indicated. For clarity, vertical offsets of 1.5 were applied to adjacent graphs.

substantial Brownian motion during the first few minutes of coarsening.

Figure 2 depicts the scaled, normalized domain radius distribution $P(R/\langle R \rangle)$ at the four different time points marked (a)–(d) in the top plot of Fig. 1. Gaussian fits are seen to provide a close approximation; the (2D version of the) Lifshitz-Slyozov universal distribution [7] is displayed as a reference [3,7,8]. Linear fits to quantile-quantile (QQ) plots (not shown), comparing the *raw* data (prior to binning) to the standard normal distribution, reveal departures from linearity only in the wings (of diminished statistical weight), while a linear correlation obtains over an interval of at least $\pm 1.5\sigma$ about the mean [14].

Accepting the Gaussian as a valid representation of the principal statistical aspects of the data [18], we are led to conclude that dynamic scaling is indeed satisfied throughout the regime of power-law growth, covering at least three decades in time. In particular, there is thus no sign of any narrowing in the distribution which would accompany the ordering transition expected to terminate coarsening in systems with competing interactions [19–22]. This conclusion is affirmed by the fact that the concentration $p(6) \equiv N_{n=6}/N$, a measure for local hexatic order in bubble patterns [23], remains constant at a low value of <0.5.

The spontaneous formation of droplet ("bubble") domains in Langmuir films of the type investigated here has been attributed to the presence of competing interactions [19], a view well supported by a variety of experiments [13,17]. The modulation period Λ_D, characterizing the ground state of these systems, sets an upper limit $\overline{R} \sim \phi^{1/2}\Lambda_D$, ϕ denoting area fraction of minority phase to the mean domain radius $\langle R \rangle$, and the condition $\langle R \rangle (t = t^*) = \overline{R}$ thus defines a characteristic crossover time t^*. Given domains of (lateral molecular) dipole density Δp and (bare) line tension γ, an estimate of t^* may be obtained [24] in the form $t^* = t_m \exp(n^{-1}\gamma/\Delta p^2)$, where $t_m \simeq 5 \times 10^{-8}$ s represents a microscopic time. With an approximate upper limit of $N_B \equiv \Delta p^2/\gamma \sim 0.14$ [13,25], and $n = 0.28$, this expression yields $t^* = t_m \exp\{[(0.28)(0.14)]^{-1}\} \sim 5 \times 10^3$ s. A slightly smaller value of N_B, determined primarily by the quench depth for given ϕ, but unfortunately not known with any precision [25], moves t^* out of reach: For example, $N_B \sim 0.12$ gives a value of $t^* \sim 5 \times 10^5$ s. We

conclude that our experiments did not reach the crossover regime [26].

The Gaussian shape of the scaled droplet radius distribution exhibits characteristic deviations from the mean-field (Lifshitz-Slyozov) solution (Fig. 2). These are generally attributed to interdomain interactions which may be diffusion mediated [3,4] or may reflect other, here possibly, dipolar contributions which are expected to induce spatial correlations in the evolving droplet domain patterns [6,8]. A suitable probe of (local) structure is the Voronoi diagram [9,23] of droplet domain centroids (Fig. 1), which facilitates evaluation of the distribution of coordination numbers $P(n)$. For the pattern in the right-hand inset of Fig. 1, we obtain typical probability densities, $p(k) \equiv N_{n=k}/N$: $p(4)$: 0.02, $p(5)$: 0.27, $p(6)$: 0.50, $p(7)$: 0.18, $p(8)$: 0.03, with second moment $\mu_2 \equiv \sum_n (n-6)^2 p(n) = 0.64$ [27]. The $p(n)$ were found to be essentially time independent, μ_2 ranging between 0.65 and 0.85.

The joint probability distribution $P(n,A)$ determines the form of the interdependence of $x_n \equiv \langle A_n \rangle / \langle A \rangle$, $\langle A_n \rangle$ denoting the mean area of n-fold coordinated *droplets* (*not* that of the corresponding n-sided Voronoi polygons) and *topological charge*, $C \equiv n - 6$. As illustrated in the inset of Fig. 3, we generally find a linear dependence of x_n, in accordance with the Lewis law of cellular patterns (froths) [9]. Linear fits by the Lewis law in the form $x_n = b + \lambda(n-6)$ give typical values $0.95 \leq b \leq 1.05$ and $0.2 \leq \lambda \leq 0.25$, with $\lambda = 0.24$ for the inset. Deviations from linearity do occur on occasion, given that statistics for x_4 and x_8 are not always reliable. More robust is the linearity in the correlation between C and the product $nm(n)$ of coordination number n of a given domain and the average coordination number $m(n)$ of the domains in its NN shell, in accordance with the Aboav-Weaire law of cellular patterns [9]. This is again illustrated in the inset of Fig. 3, yielding a value of $a \simeq 1.1$ for the constant in the Aboav-Weaire law in the form $nm(n) = (6-a)(n-6) + b$, with [9] $b = \sum_n nm(n)p(n) = 36 + \mu_2$. These linear correlations indicate an unexpected, close analogy between disordered droplet patterns and space filling cellular patterns (froths). Specifically, the values we obtain for the three parameters μ_2, λ, and a are virtually identical to those of equilibrated random Voronoi lattices [9,28].

To ascertain correlations in the areas assumed by adjacent domains [6,8], we display, as in Fig. 3, for each domain of area A in a given pattern, the average area of its nearest neighbors $\langle A \rangle_{\mathrm{NN}}$ relative to A. Pronounced anticorrelations are apparent: For domains of smaller than average area A, $\langle A \rangle_{\mathrm{NN}}$ exceeds A and vice versa. While this observation is entirely consistent with the prediction of "direct" correlations between domains, based on the analysis of the domain coarsening dynamics [3,6,8]. We note that such anticorrelations represent a quintessential property of space filling cellular structures. Their evolution has been shown [29] to proceed via configurations which maximize the entropy $S \sim -\sum_n \int dA\, P(n,A) \ln(P(n,A))$, under a set of constraints whose interrelation produces the Lewis law

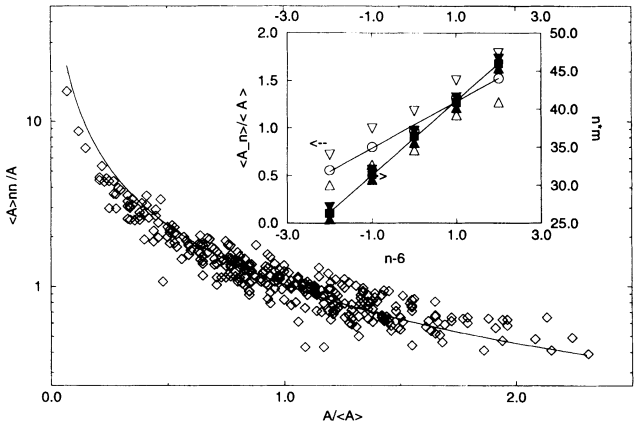

FIG. 3. Area correlations between NN domains. Spatial correlations in the area values assumed by adjacent domains for the right-hand inset of Fig. 1. The solid line represents the model discussed in the text. Inset: Plots (with linear fits) corresponding to Lewis law (open circles, left ordinate) and Aboav-Weaire law (solid squares, right ordinate), as discussed in the text, where $\langle A \rangle_{nn}$, $\langle A \rangle$, $\langle A_n \rangle$, n, and m are defined. Open and solid triangles indicate $\pm 1/2$ standard deviation for Lewis and Aboav-Weaire plots, respectively.

[9] and the Aboav-Weaire law [30]. A recent generalization of maximum entropy analysis to disordered droplet patterns [31,32] does in fact produce a functional form of $P(R/\langle R \rangle)$, which closely matches a Gaussian. In addition, it generates an explicit expression [33], $f = f(\mu_2, \lambda, a)$, for the requisite relation between the quantities plotted in Fig. 3: The solid line shown there employs the independently obtained values $\mu_2 = 0.64$, $\lambda = 0.25$, $a = 1.1$, without (additional) adjustable parameters.

The remarkably accurate reproduction of the local pattern structure, generated by the "packing" of domains of differing size, is a consequence of the virtually complete screening of topological charge at the NN level: That is, topological charges are essentially "associated" into neutral NN clusters [31]. From this point of view, correlations in the domain areas simply reflect correlations between topological defects. As first noted by Magnasco, the relaxation of domains, via area adjustment, into this type of optimized local packing in fact generates a well-defined topology [34]. Evaluation of the ("discrete") charge correlation function $\langle \sum_{j \epsilon k\mathrm{NN}} C(0)C(j)/N_{k\mathrm{NN}} \rangle$, with k denoting the index of the kth NN shell (and thus representing topological distance), in fact demonstrates that correlations decay from $\sim \mu_2$ at $k = 0$, to $\sim -\mu_2/4$ at $k = 1$ and to less than $\sim \mu_2/100$ at $k = 2$ [31].

The locally optimal domain packing must be stabilized against domain coalescence, and it is here that repulsive electrostatic interactions between domains are most likely to come into play. The configurations adopted by our droplet patterns exhibit a preferred distance of closest approach s_{ij} between boundaries of adjacent domains i and j, producing a pronounced peak in the distribution [34] $P(s_{ij}/\langle s_{ij} \rangle)$ whose shape is in fact preserved throughout the power-law growth regime [14].

We suggest that it is the combination of charge screening and local stabilization against droplet coalescence which generates the observed equivalence of our droplet pattern topology to that of *equilibrated* random Voronoi lattices. It appears natural to assume that there is no specific requirement as to the precise distance dependence of the (repulsive) interaction, so long as domain fusion is suppressed. Consequently, the spatial correlations described here may be expected in a wide range of systems in which such interactions may occur, with a potentially quite general role of entropy maximization in the selection of pattern configurations.

The work presented here has benefited from the advice of Colin Mallows and John Marko.

*Permanent address: Department of Physics, M.I.T., Cambridge, MA 01238.

†Permanent address: Laboratoire de Physique Quantique, Université Paul Sabatier, 31062 Toulouse, Cedex, France.

[1] For reviews, see: J. D. Gunton, M. San Miguel, and P. S. Sahni, in *Phase Transitions and Critical Phenomena*, edited by C. Domb and J. L. Lebowitz (Academic Press, New York, 1983) Vol. 3; S. Komura, Phase Transitions **12**, 3 (1988).

[2] I. M. Lifshitz and V. V. Slyozov, J. Phys. Chem. Solids **19**, 35 (1961); C. Wagner, Z. Elecktrochem. **65**, 581 (1961).

[3] P. W. Voorhees, J. Stat. Phys. **38**, 231 (1985); N. Akaiwa and P. W. Voorhees (to be published).

[4] T. Imaeda and K. Kawasaki, Physica (Amsterdam) **164A**, 335 (1990).

[5] J. A. Marqusee and J. Ross, J. Chem. Phys. **80**, 536 (1984); J. A. Marqusee, *ibid.* **81**, 976 (1984).

[6] M. Marder, Phys. Rev. A **36**, 438 (1987); Q. Zheng and J. D. Gunton, Phys. Rev. A **39**, 4848 (1989); H. Hayakawa and F. Family, Physica (Amsterdam) **163A**, 491 (1990).

[7] T. M. Rogers and R. C. Desai, Phys. Rev. B **39**, 11 956 (1989).

[8] O. Krichevsky and J. Stavans, Phys. Rev. Lett. **70**, 1473 (1993).

[9] D. Weaire and N. Rivier, Contemp. Phys. **25**, 59 (1984); H. Flyvbjerg, Phys. Rev. E **47**, 4037 (1993).

[10] D. J. Benvegnu and H. M. McConnell, J. Phys. Chem. **96**, 6820 (1992).

[11] An excluded volume effect increases the nominal value of ϕ by ~30%.

[12] C. L. Hirshfeld and M. Seul, J. Phys. (Paris) **51**, 1537 (1990).

[13] M. Seul and M. J. Sammon, Phys. Rev. Lett. **64**, 1903 (1990); M. Seul, J. Phys. Chem. **97**, 2941 (1993); M. Seul and V. S. Chen, Phys. Rev. Lett. **70**, 1658 (1993).

[14] N. Y. Morgan and M. Seul (to be published).

[15] The observation of a growth exponent $n < \frac{1}{3}$ is in accord with simulations of model B [7]: Logarithmic corrections, relevant in 2D, account for the slow approach to the asymptotic value of $\frac{1}{3}$. The derivative $d \ln\langle R\rangle/d \ln t$ does not indicate any time-dependent changes in n.

[16] Marqusee, Eq. 4.1, second entry in [5], obtains $k = a_0[2(\gamma/kT)DA^2\bar{c}(\infty)]^{1/3}$. With estimates of the (bare) line tension $\gamma \simeq 10^{-7}$ dyne, the diffusion constant $D \simeq 5 \times 10^{-8}$ cm^2/s, the molecular area within the minority phase $A \simeq 80$ Å, and the equilibrium concentration in the bulk of the majority phase $\bar{c}(\infty) \simeq 1/40$ Å [10,12,13], and with a numerical correction factor $a_0(\phi \simeq 0.25) \simeq 0.8$, one finds $k \simeq 0.3$ μm/min$^{1/3}$.

[17] H. M. McConnell, Annu. Rev. Phys. Chem. **42**, 171 (1991); K. Y. Lee, J. F. Klingler, and H. M. McConnell, Science **263**, 655 (1994).

[18] Prior to binning, the (raw) data consistently produce a small positive value for the third moment (skewness) which is more pronounced for lower values of ϕ [14].

[19] D. Andelman, F. Brochard, and J. F. Joanny, J. Chem. Phys. **86**, 3673 (1987).

[20] C. Sagui and R. C. Desai, Phys. Rev. Lett. **71**, 3995 (1993); Phys. Rev. E **49**, 2225 (1994).

[21] M. Bahiana and Y. Oono, Phys. Rev. A **41**, 6763 (1990).

[22] L. Q. Chen and A. G. Khachaturyan, Phys. Rev. Lett. **70**, 1477 (1993).

[23] M. Seul and C. A. Murray, Science **262**, 558 (1993); M. Seul, J. Phys. I (France) **4**, 319 (1994).

[24] J. F. Marko (private communication). Mass balance at the interface of a domain growing at the rate dR/dt in response to a material flux driven by the gradient in the chemical potential, $\mu \sim \gamma/R - \Delta p^2 \ln(R/d)/R$, implies $dR/dt \sim -\nabla\mu$. In equilibrium, $dR/dt = 0$, and $\bar{R} \simeq d\exp(\Delta p^2/\gamma)$ [17]. Equating $\bar{R}$ with $(D\xi t^*)^n$ produces the desired expression for t^*; $t_m \equiv d^3/D\xi$ is a microscopic time set by a molecular length ("cutoff") $d \sim 5$ Å, the diffusion constant $D \sim 5 \times 10^{-8}$ cm^2/s, and the interface width $\xi \sim d$, yielding $t_m \simeq 5 \times 10^{-8}$ s.

[25] R. E. Goldstein and D. Jackson, J. Phys. Chem. (to be published).

[26] Linear stability analysis indicates the existence of a threshold in the coupling constant N_B of dipolar interactions to ensure stability of the $q = 0$ mode when crossing the phase boundary. This threshold appears to increase as the thickness d of a dipolar sheet decreases [20]. It is conceivable that our experiments are in fact governed by an entire band of unstable modes in the range $q = 0$ to $q \sim \Lambda_D^{-1}$.

[27] The densities $p(n)$ strictly satisfy the Euler-Poincaré identity $\sum_n (n - 6)p(n) = 0$, only in the limit of infinite system size; the imbalance we observe is typical of edge effects in the Voronoi construction.

[28] K. Baekgaard Lauritsen, C. Moukarzel, and H. J. Herrmann, J. Phys. I (France) **3**, 1941 (1993).

[29] N. Rivier, J. Phys. (Paris) Colloq. **43**, C9–91 (1982); N. Rivier and R. Lissowski, J. Phys. A **15**, L143 (1982).

[30] M. A. Peshkin, K. J. Strandburg, and N. Rivier, Phys. Rev. Lett. **67**, 1803 (1991).

[31] C. Sire and M. Seul, J. Phys. I (France) (to be published).

[32] A monotonic (essentially linear) correlation obtains between areas of droplets A and areas of corresponding Voronoi polygons A_{Vp}, with $\langle A\rangle/\langle A_{Vp}\rangle = \phi$. This relation also gives strong evidence for an excluded volume effect [11,31].

[33] With $n(x) = 6 + (x - 1)/\lambda$, in accordance with the Lewis law, and $x \equiv A/\langle A\rangle$, the function $f = f(\mu_2, \lambda, a)$ has the explicit form [31] $f = \{1 + [a(1 - x) + \lambda\mu_2]/n(x)\}/x$.

[34] Specifically, this implies the existence of a well-defined Voronoi diagram for polydisperse droplets (not just for their centroids). M. O. Magnasco, Philos. Mag. **65**, 895 (1992).

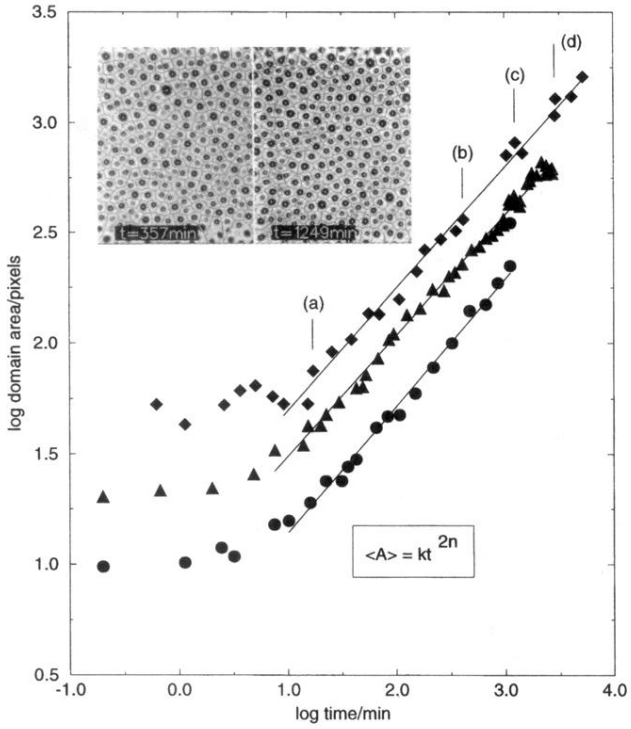

FIG. 1. Domain coarsening. Temporal evolution of mean domain area $\langle A \rangle$ for three runs at composition 80:20, corresponding to $\Phi \sim 0.25$, at temperature 19 °C and approximate surface pressure $\pi \simeq 6$ dyn/cm. Vertical offsets were applied to the middle (-0.25) and bottom (-0.50) graphs. The conversion factor for area units is 10 pixels $\equiv$ 12.4 μm^2. Solid lines represent linear fits which determine the growth exponent (see text). Labels (a)–(d) refer to respective graphs in Fig. 2 below. Inset: Snapshots of (portions of flat-fielded [14]) domain patterns at different stages of coarsening taken from the run, corresponding to the top plot; the corresponding Voronoi diagrams are superimposed. Note the different scales: the black label box represents 150 μm (left panel) and 240 μm (right panel), respectively.